SCIENCE CHINA
Chemistry

• ARTICLES •
• SPECIAL TOPIC • Molecular Functional Materials and Applications

June 2016 Vol.59 No.6: 713–718
doi: 10.1007/s11426-016-5597-9

Activated pyrolysed bacterial cellulose as electrodes for supercapacitors

Xiangjun Wang[1,3], Debin Kong[2], Bin Wang[2], Yan Song[1*] & Linjie Zhi[2*]

[1]*Key Laboratory of Carbon Materials; Institute of Coal Chemistry, Chinese Academy of Sciences, Taiyuan 030001, China*
[2]*CAS Key Laboratory of Nanosystem and Hierarchical Fabrication; CAS Center for Excellence in Nanoscience, National Center for Nanoscience and Technology, Beijing 100190, China*
[3]*University of Chinese Academy of Sciences, Beijing 100049, China*

Received December 30, 2015; accepted January 19, 2016; published online April 20, 2016

In this paper, the bacterial celluloses (BCs) were pyrolysed in nitrogen and then activated by KOH to form a porous three-dimension-network electrode material for supercapacitor applications. Activated pyrolysed bacterial cellulose (APBC) samples with enlarged specific surface area and enhanced specific capacitances were obtained. In order to optimize electrochemical properties, APBC samples with different alkali-to-carbon ratios of 1, 2 and 3 were tested in two electrodes symmetrical capacitors. The optimized APBC sample holds the highest specific capacitance of 241.8 F/g, and the energy density of which is 5 times higher than that of PBC even at a current density of 5 A/g. This work presents a successful practice of preparing electrode material from environment-friendly biomass, bacterial cellulose.

bacterial cellulose, pyrolysis, activation, supercapacitor

Citation: Wang XJ, Kong DB, Wang B, Song Y, Zhi LJ. Activated pyrolysed bacterial cellulose as electrodes for supercapacitors. *Sci China Chem*, 2016, 59: 713−718, doi: 10.1007/s11426-016-5597-9

1 Introduction

The tremendous growth of portable electronic devices and electric vehicles has highly promoted the demand for high-power energy storage devices. Supercapacitors are considered as promising high power and long-life devices. Carbon, especially with high surface area and high electro conductivity, is one kind of important electrode materials for supercapacitors, because of their electrical conductivity, chemical stability and low cost. However, the sources of carbon materials usually come from non-renewable fossil fuel. Thus, for the sustainable development, some renewable biomaterial has emerged as the replacement of the fossil fuel as the sources of carbon electrode materials, such as crab shell [1,2], chicken eggshell membranes [3], egg white [4], chicken feather [5] and silk [6,7]. But, this kind of animal biomaterial is either expensive, or hard to pretreat. Besides the animal material, some relatively low-cost plants, such as leaves [8–10], nuts shells [11–16], stem [17,18] and various pollens [19], are also attractive, whereas their yields are seasonal and some of them are inconvenient to collect. Fortunately, bacterial celluloses (BCs), the specific product of primary metabolism of plant biomass, could be produced easily and massively by the bacteria of genera Acetobacter [20]. Moreover, BCs happen to have ultrafine reticulated structure formed with ribbon-shaped nanofibers naturally. The net-like structure allows BCs with sufficient porosity and high specific surface area, which corresponds to the properties of carbon electrode materials mentioned above. Accordingly, BCs and their derivatives have attracted great scientific interest as the alternatives to replace the previ-

*Corresponding authors (email: yansong1026@126.com; zhilj@nanoctr.cn)

ously existing carbon source of the supercapacitors electrode materials.

Recently, pyrolysed bacterial cellulose (PBC), pyrolysed BCs, began to be studied as the electrode material of the supercapacitors due to its high electro-conductivity and nano-porous architecture [21–23]. Unfortunately, the specific surface area of PBC physically activated with CO_2 is only 166 m^2/g, much lower than commercial activated carbon, and the electrochemical capacitance is as low as 42 F/g [23]. It is well known that the specific surface area as well as the pore size distribution of carbon electrodes affects the performance of the resulting capacitance. Consequently, the specific surface area and pore structure of PBC is highly required to be improved for the enhancement of the electrochemical capacitance. Chemical activation with alkali compounds such as KOH and NaOH is a well-known method to activate carbon materials with a high surface area and controllable pore size [24,25].

Herein, we activated PBC with potassium hydroxide (KOH), and the mass ratios of KOH and PBC (alkali-to-carbon ratios) ranged from 1 to 3, which were denoted as APBC-1, APBC-2, and APBC-3, respectively. The electrochemical properties of PBC and activated pyrolysed bacterial cellulose (APBC) samples were tested in coin-type supercapacitors with 6 M KOH aqueous as electrolyte. The structure characteristics demonstrated that the activation degrees were amplified with the increase of the alkali-to-carbon ratios. Electrochemical properties show that APBC-1 has the highest specific capacitance and power densities.

2 Experimental

Bacterial cellulose (BC) pellicles were friendly supplied by Hainan Nanye Industry Company (China). The purification was carried out to remove the bacteria and their residues. The obtained BC pellicles were first washed by distilled water at 70 °C for 3 h, then washed in 0.1 M aqueous NaOH at 70 °C for 90 min, and thoroughly washed in distilled water until neutral pH was reached.

To maintain the morphology and the three-dimensional structure of BC, the freeze drying technology was employed. The BC pellicles were frozen in liquid nitrogen, followed by vacuum dying at −54 °C for 48 h. Then the obtained freeze-dried BC aerogel was pyrolysed under flowing argon to get pyrolysed BC (namely, PBC). Briefly, there were four temperature stages at 180, 230, 520, 900 °C respectively and 1 h at each stage. The APBC was obtained by activating with KOH as an activation agent during the following carbonization process. After sufficient mixing, the KOH/PBC slurry was prepared at 120 °C for 48 h in air, and then heated in tubular resistance furnace at a heating rate of 5 °C/min from room temperature to 900 °C. Finally, the etched products were washed, and dried in vacuum at 60 °C for 24 h.

The scanning electron microscopy (SEM) micrographs were obtained using a Hitachi S4800 instrument (Japan). The transmission electron microscopy (TEM) micrographs were obtained using an FEI Tecnai F20 instrument (USA) operating at 200 kV. Raman spectra were collected using an inVia Raman microscope (Renishaw, UK) with a laser wavelength of 514.5 nm. X-ray photoelectron spectroscopy (XPS) measurement was carried out on an ESCALAB250Xi apparatus at base pressure of 1×10^{-9} mbar, and X-ray source of Al Kα. The nitrogen adsorption was measured using a Micromeritics accelerated surface area porosimetry (ASAP 2020, USA) auto adsorption analyzer to obtain N_2 adsorption isotherms at 77 K, and the specific surface area (SSA) was obtained by Brunauer-Emmett-Teller (BET) analyses of the adsorption isotherms.

The electrochemical comparison of PBC and APBC were carried out by the two-electrode symmetric supercapacitor systems, where two electrodes with exactly the same composition and mass were separated by glass fiber soaked with 6 M KOH aqueous solutions, and then assembled into coin-type cells. All of the cyclic voltammetry (CV) measurements were performed using a CHI660D electrochemical station (CH Instrument, Shanghai, China). The galvanostatic charge/discharge measurements were made using a CT2001A Battery Program Controlling Test System (China-Land Com. Ltd.) within the voltage range from 0 to 1 V.

The specific capacitance (C_s) was calculated according to the equation:

$$C_s = 2\times\frac{I\Delta t}{m\Delta U}$$

where I (A) is the discharge current, Δt (s) is the discharge time, m (g) is the weight of the active material in an individual electrode, and ΔU (V) is the discharge voltage.

3 Results and discussion

Purification by aqueous sodium hydroxide was employed to remove the bacteria residue. Freeze-drying worked by freezing water-saturated BCs and then reducing the surrounding pressure around the nanoribbons to allow the frozen water to sublimate directly from the solid phase to the gas phase. Then the three-dimensional structure of BCs were maintained effectively by the freeze drying (Scheme 1). As shown in Figure 1, the dehydrated BCs nanoribbons naturally form a net structure with various pores and linkage between the adjacent parts, which provide possibilities for the ion transportation, while another basic requirement of the electrode materials of supercapacitors is electrical conductivity. Accordingly, BCs were pyrolysed at 900 °C in the absence of oxygen to improve the electronic conductivity. Activation by KOH was employed to increase the specific

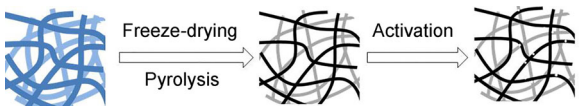

Scheme 1 Scheme of the preparation of APBC (color online).

surface area and optimize the pore structure.

3.1 Morphology characterization

Figure 1(a) depicted the scanning electron microscope (SEM) image of BCs after freeze-drying. The porous networks consisted of straight nanoribbons. The process of pyrolysis not only decreased the width of the nanoribbons, but maintained the three-dimensional porous architectures of PBC (Figure 1(b)). It is obvious that the diameter of PBC nanoribbons is approximately 20 nm according to transmission electron microscope (TEM) images of PBC (Figure 1(c)). The inset of Figure 1(c) depicted the concentric diffraction rings of PBC indicating the graphite-like structure. Moreover, the specific surface area and the pore distributions are the key factors to the electrochemical properties. The activation, especially by potassium hydroxide (KOH), is an effective way to increase the surface area and porosity for carbon materials [26,27]. Activation partially destroyed the original three-dimensional structure of the PBC, which shortened the distance of the nanoribbons and reduced the number of the macrospores (Figure 1(d, e)). In addition, the activation formed micropores under 10 nm on the nanoribbons of APBC (Figure 1(f)), while the graphite degree of APBC was weaker compared with that of PBC (the inset of Figure 1(c)).

The Fourier transform infrared spectroscopy (FTIR) analysis was performed to determine the functional groups, especially the oxygen-containing groups. The FTIR spectra of the materials before and after activation are shown in Figure 2(a). The FTIR image showed the similar peak positions and shapes among PBC, APBC-1, APBC-2 and APBC-3 samples. The peak positions of IR images (Figure 2(a)) showed the functional groups of PBC and APBC samples. As the activation degree increased, the FTIR intensity of APBC samples showed gradual increases at characteristic peaks of the oxygen-containing groups, especially at the wavenumbers of 1604 and 1158 cm^{-1}. Accordingly, the activation increased the surface oxygen-containing groups, such as C–O and C=O. The results of the XPS C1s tests are shown in Figure 2(b). The deconvolution of PBC C1s spectrum yields two peaks. The main peak at 284.8 eV is somewhat associated to sp^2 C in the PBC nanofibrils considering the presence of graphitic layers [28]. The relatively weak peak at 285.6 is assignable to carbon atoms in C=O, suggesting that there exist a small portion of oxygen-containing functional groups in the thus-prepared PBC nanofibrils. The C1s spectra of APBC-1, APBC-2 and APBC-3 show nearly the same figures as that of PBC. The original sp^2 characteristic peaks and C=O peaks at 284.8 and 285.6 eV are retained for APBC samples, whereas the half peak widths narrowed in small increments as the activation. Table S1 (Supporting Information online) summarizes the elemental compositions (at%) on the surface of PBC and APBC samples or over the sampling depth of several atomic layers from the surface. The oxygen content increased with the increase of the activation, which agreed with the FTIR intensity increasing.

KOH activation was effective to improve the porosity of PBC while its original fibrous form was sustained. Figure 3 depicts BET nitrogen adsorption-desorption isotherm of the PBC and APBC samples at 77 K. In the low pressure region, the adsorption quantities of the APBC samples were much higher than that of PBC, indicating that the activation formed more micropores. It can be seen that the PBC and APBC-1 isotherms represented a type IV isotherm with H4

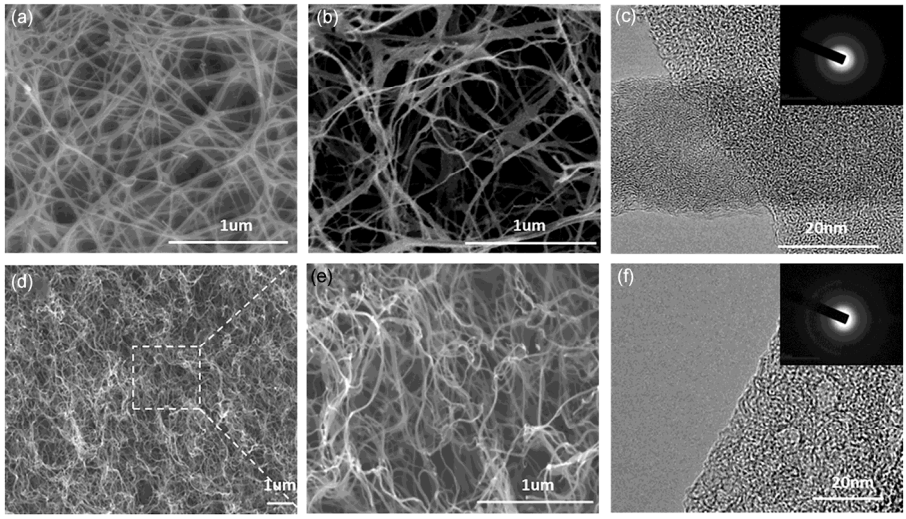

Figure 1 Morphologies and characteristics of BC, PBC and APBC. (a) SEM image of BC; (b) SEM image of PBC; (c) TEM image of PBC; (d, e) SEM images of APBC; (f) TEM image of APBC.

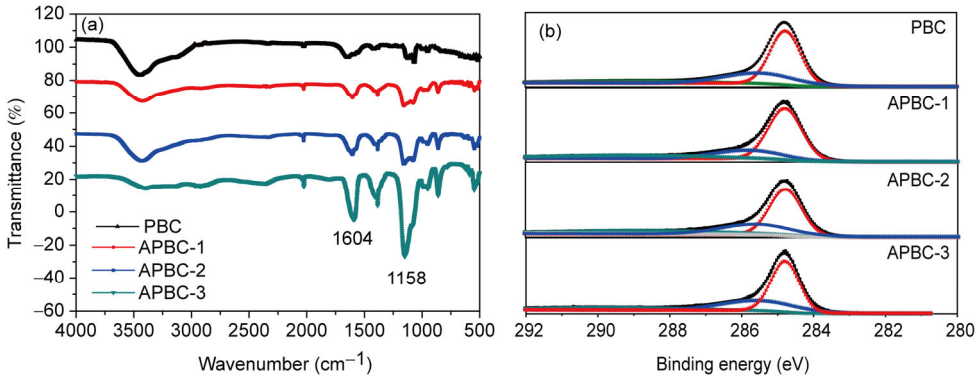

Figure 2 FTIR spectra (a) and XPS C1s spectra (b) of PBC and APBC (color online).

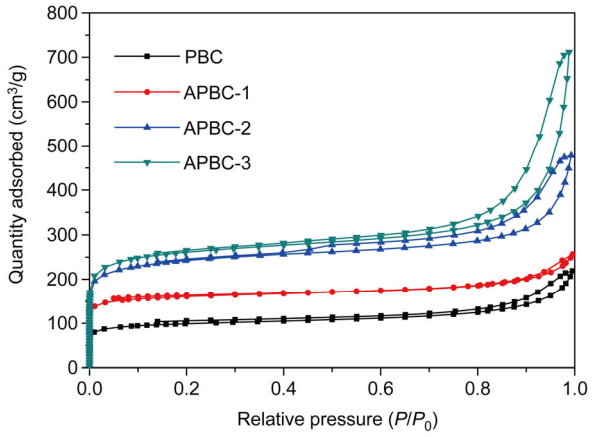

Figure 3 Nitrogen adsorption-desorption isotherm of PBC, APBC-1, APBC-2 and APBC-3 (color online).

type hysteresis loop, which were bimodal distributions of micropores and mesopores [29,30]. The high pressure hysteresis and the loop of APBC-2 and APBC-3 samples showed H3 type hysteresis loop, indicating the similar pore structures, but larger sizes than that of PBC and APBC-1. The BET specific surface area and pore-structure parameters of PBC and APBC samples are illustrated in Table S2. The specific surface areas measured in accordance with the standard BET method were 337, 491, 829 and 892 m^2/g respectively for PBC, APBC-1, APBC-2 and APBC-3. It can be seen that the effect of KOH dosage on the specific surface area of APBC samples is apparent. However, APBC-1, with the alkali and carbon ratio of 1, has the minimum values of S_{mic}/S_e (the ratio of the microspores surface area and the external surface area) and the average pore diameter.

3.2 Electrochemical performance

Figure 4(a) exhibits the cyclic voltammetry (CV) curves of PBC, APBC-1, APBC-2, and APBC-3 electrodes between 0 and 1 V at the scan rate of 100 mV/s. The CV curves showed typical rectangular shapes, indicating highly capacitive nature with very rapid charge/discharge characteristics [31,32]. The APBC-1 electrode provides the supercapacitor with an energy density of 38 W h/kg at a current density of 0.1 A/g and improves the rate performance as well. At a current density of 5 A/g, it can still deliver an energy density of 15 W h/kg, which is nearly 5 times higher than that of PBC-based supercapacitors. APBC-1 electrodes showed superior specific capacitances at current densities ranging from 0.1 to 5 A/g, compared with the other electrodes (Figure 4(b)). Specially, the specific capacitance of the APBC-1 electrode reached 241.8 F/g at a current density of 0.1 and 167.4 F/g at a current density of 1 A/g, respectively. Accordingly, the proportion and the size of the mesopores are the keys to the performance of the capacitance, but not the functional group. Therefore, the electrode material in the supercapacitor works as a double layer capacitor electrode rather than a pseudocapacitor electrode. The APBC-1 electrode provided the supercapacitor with an energy density of 38 W h/kg at a current density of 0.1 A/g and 15 W h/kg at 5 A/g, which is nearly 5 times higher than that of PBC-based supercapacitors (Figure 4(c)). Moreover, with the increase of the power densities, the descending slope of APBC-1 is the smallest, indicating the fast charge and discharge properties. Additionally, all the four kinds of supercapacitors showed over 90% capacitance retention even after 10000 charge-discharge cycles (Figure 4(d)). Thus, APBC-1 served as an excellent electrode material for higher specific capacitance and high-power supercapacitors with long-life.

4 Conclusions

Activation by KOH was employed to prepare activated three-dimensional network carbons originating from bacterial cellulose. APBCs with enlarged specific surface area and enhanced specific capacitances were obtained. Among the APBC samples, APBC-1, with alkali-to-carbon ratio of 1, has the highest specific capacitance of 241.8 F/g. More importantly, APBC-1 maintains 15 W h/kg at a current density

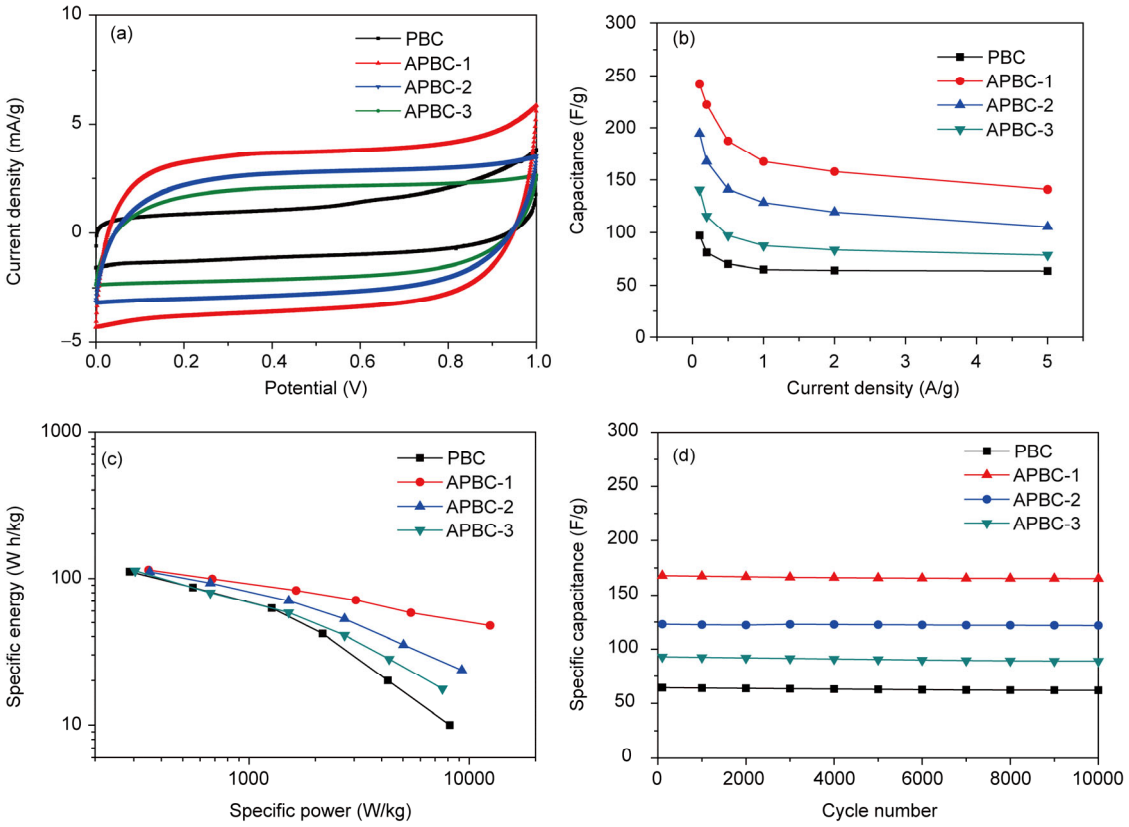

Figure 4 Electrochemical performances of supercapacitors. (a) Cyclic voltammetry curves; (b) specific capacities at various current densities; (c) Ragone plots; (d) cycling capabilities of PBC, APBC-1, APBC-2 and APBC-3 (color online).

of 5 A/g which is nearly 5 times higher than that of PBC, highlighting the promise of this novel material for high power supercapacitor applications. This work presents a successful practice of preparing electrode material from environment-friendly biomass, bacterial cellulose.

Acknowledgments This work was supported by the Ministry of Science and Technology of China (2012CB933403), the National Natural Science Foundation of China (21173057, 51425302), and the Chinese Academy of Sciences.

Conflict of interest The authors declare that they have no conflict of interest.

Supporting information The supporting information is available online at http://chem.scichina.com and http://link.springer.com/journal/11426. The supporting materials are published as submitted, without typesetting or editing. The responsibility for scientific accuracy and content remains entirely with the authors.

1 Wang H, Zhu E, Yang J, Zhou P, Sun D, Tang W. *J Phys Chem C*, 2012, 116: 13013–13019
2 Wang H, Bian L, Zhou P, Tang J, Tang W. *J Phys Chem A*, 2012, 1: 578–584
3 Li Z, Zhang L, Amirkhiz BS, Tan X, Xu Z, Wang H, Olsen B, Holt C, Mitlin D. *Adv Eng Mater*, 2012, 2: 431–437
4 Li Z, Xu Z, Tan X, Wang H, Holt C, Stephenson T, Olsen B, Mitlin D. *Energy Environ Sci*, 2013, 6: 871–878
5 Wang Q, Cao Q, Wang XY, Jing B, Kuang H, Zhou L. *J Power Sources*, 2013, 225: 101–107
6 Kim YJ, Abe Y, Yanaglura T, Park K, Shimizu M, Iwazaki T, Nakagawa S, Endo M, Dresselhaus M. *Carbon*, 2007, 45: 2116–2125
7 Yun YS, Cho SY, Shim J, Kim B, Chang S, Baek S, Huh Y, Tak Y, Park Y, Park S, Jin H. *Adv Mater*, 2013, 25: 1993–1998
8 Wang R, Wang P, Yan X, Lang J, Peng C, Xue Q. *ACS Appl Mater Interf*, 2012, 4: 5800–5806
9 Uchiyama S, Tamata M, Tofuku Y, Suzuki S. *Anal Chim Acta*, 1988, 208: 287–290
10 Biswal M, Banerjee A, Deo M, Ogale S. *Energy Environ Sci*, 2013, 6: 1249–1259
11 Rufford TE, Hulicova-Jurcakova D, Zhu Z, Lu GQ. *Electrochem Commun*, 2008, 10: 1594–1597
12 Guo PZ, Ji QQ, Zhang LL, Zhao SY, Zhao XS. *Acta Physico-Chimica Sinica*, 2011, 27: 2836–2840
13 He X, Ling P, Qiu J, Yu M, Zhang X, Yu C, Zheng M. *J Power Sources*, 2013, 240: 109–113
14 Valente Nabais JM, Teixeira JG, Almeida I. *Bioresour Technol*, 2011, 102: 2781–2787
15 Sun L, Tian C, Li M, Meng X, Wang L, Wang R, Yin J, Fu H. *J Mater Chem A*, 2013, 1: 6462–6470
16 Elmouwahidi A, Zapata-Benabithe Z, Carrasco-Marín F, Moreno-Castilla C. *Bioresour Technol*, 2012, 111: 185–190
17 Liu X, Zheng M, Xiao Y, Yang Y, Yang L, Liu Y, Lei B, Dong H, Zhang H, Fu H. *ACS Appl Mater Interf*, 2013, 5: 4667–4677
18 Fan Z, Qi D, Xiao Y, Yan J, Wei T. *Mater Lett*, 2013, 101: 29–32
19 Zhang L, Zhang F, Yang X, Leng K, Huang Y, Chen Y. *Small*, 2013, 9: 1342–1347
20 Jonas R, Farah LF. *Polym Degrad Stabil*, 1998, 59: 101–106
21 Chen LF, Huang ZH, Liang HW, Yao WT, Yu ZY, Yu SH. *Energy*

Environ Sci, 2013, 6: 3331–3338
22 Chen LF, Huang ZH, Liang HW, Guan Q, Yu S. *Adv Mater*, 2013, 25: 4746– 4752
23 Lee KY, Qian H, Tay FH, Blaker JJ, Kazarian SG, Bismarck A. *J Mater Sci*, 2013, 48: 367–376
24 Yoon SH, Lim S, Song Y, Ota Y, Qiao W, Tanaka A, Mochida I. *Carbon*, 2004, 42: 1723–1729
25 Wen ZB, Qu QT, Gao Q, Zheng X, Hu Z, Wu Y, Liu Y, Wang X. *Electrochem Commun*, 2009, 11: 715–718
26 Zhai Y, Dou Y, Zhao D, Fulvio PF, Mayes RT, Dai S. *Adv Mater*, 2011, 23: 4828–4850
27 Frackowiak E, Beguin F. *Carbon*, 2001, 39: 937–950
28 Wang B, Li X, Luo B, Yang J, Wang X, Song Q, Chen S, Zhi L. *Small*, 2013, 9: 2399–2404
29 Serilevy A, Avnir D. *Langmuir*, 1993, 9: 3067–3076
30 Sing KSW. *Adv Colloid Interface Sci*, 1998, 76: 3–11
31 Kotz R, Carlen M. *Electrochim Acta*, 2000, 45: 2483–2498
32 Wang G, Zhang L, Zhang J. *Chem Soc Rev*, 2012, 41: 797–828